



## Effects of cooling rate on bio-corrosion resistance and mechanical properties of Mg–1Zn–0.5Ca casting alloy

Li-dong WANG<sup>1,2</sup>, Xue-song LI<sup>3</sup>, Chao WANG<sup>3</sup>, Li-min WANG<sup>2</sup>, Zhan-yi CAO<sup>1</sup>

1. Key Laboratory of Automobile Materials, Ministry of Education, Department of Materials Science and Engineering, Jilin University, Changchun 130025, China;
2. State Key Laboratory of Rare Earth Resource Utilization, Changchun Institute of Applied Chemistry, Chinese Academy of Sciences, Changchun 130022, China;
3. Key Laboratory of Advanced Structural Materials, Ministry of Education, Changchun University of Technology, Changchun 130012, China

Received 18 May 2015; accepted 17 November 2015

**Abstract:** Mg–1Zn–0.5Ca alloys were prepared by traditional steel mould casting and water-cooled copper mould injection casting at higher cooling rate. Microstructure, mechanical properties and bio-corrosion resistance of two alloys were contrastively investigated. Grain size reduces remarkably and microstructure becomes homogenous when raising cooling rate. The bio-corrosion behaviour in 3.5% sodium chloride solution (3.5% NaCl) and Hank's solution at 37 °C was investigated using electrochemical polarization measurement and the results indicate that the alloy prepared at higher cooling rates has better corrosion resistance in both types of solution. Further mass loss immersion test in Hank's solution reveals the same result. The reason of corrosion resistance improvement is that raising cooling rate brings about homogeneous microstructure, which leads to micro-galvanic corrosion alleviation. The tensile test results show that yield strength, ultimate tensile strength and elongation are improved by raising cooling rate and the improvement is mainly due to grain refinement.

**Key words:** Mg–1Zn–0.5Ca alloy; cooling rate; bio-corrosion resistance; micro-galvanic corrosion; mechanical properties

### 1 Introduction

Mg and its alloys have been investigated as implant materials for almost two centuries, including the AE21, AM60, WE43 and Mg–RE [1,2], because of good biocompatibility and biodegradation in the bio-environment, excellent mechanical properties such as specific strength and elastic modulus which are similar to human bone [3]. Since Ca is a major component of human bone and Zn is an essential element in the human body, Mg–Ca [4], Mg–Zn [5,6] and Mg–Zn–Ca [7] alloys have attracted researchers' attention and become a hot-button issue for a very long period. However, the main demerits of these alloys as implant materials consist of their poor corrosion resistance and mechanical properties which are not beneficial to their clinical applications. Mechanical

properties Mg–Zn–Ca alloy can be improved by heat treatment and extrusion [8]. Surface modification is an effective approach to reduce the bio-corrosion rate such as fluoride treatment [9], alkaline heat treatment [10] and hydroxyapatite coating deposition [11].

Raising cooling rate is an important method in materials preparation process. Some previous studies [12–14] investigated the effect of cooling rate on corrosion behavior and mechanical properties of Mg alloys and results show that raising cooling rate can enhance mechanical properties and corrosion resistance. It is found that raising cooling rate can bring about microstructural refinement and homogeneity, and increase the solid solubility of alloying elements into the magnesium matrix. Additionally, microstructural refinement and homogeneity could lead to chemical homogeneity, which in turn enhanced corrosion

**Foundation item:** Project (20921002) supported by the Innovative Research Groups of the National Natural Science Foundation of China; Project (21221061) supported by the National Natural Science Foundation of China; Project (201105007) supported by the Science and Technology Program of Jilin Province, China; Project (20140325003GX) supported by the Science and Technology Support Project of Jilin Province, China

**Corresponding author:** Li-dong WANG; Tel: +86-431-85262592; Fax: +86-431-85262836; E-mail: [ldwang@ciac.ac.cn](mailto:ldwang@ciac.ac.cn)  
DOI: 10.1016/S1003-6326(16)64182-1

resistance [13,14]. However, bio-corrosion behavior and mechanical properties of low alloyed Mg–Zn–Ca alloy system prepared at high cooling rate have been rarely reported. In this work, Mg–1Zn–0.5Ca alloy was prepared at high cooling rate, and then its microstructure, mechanical and bio-corrosion properties were studied compared with traditional casting alloy. The aim is to explore the effects of cooling rate on bio-corrosion resistance and mechanical properties of Mg–1Zn–0.5Ca alloy.

## 2 Experimental

Commercially pure 99% Mg, high-purity 99.99% Zn and 99.9% Ca (mass fraction) were used to prepare Mg–Zn–Ca alloys. Mg ingot was melted at 953 K in a resistance furnace under protection of an anti-oxidizing flux and then calculated amounts of Zn and Ca (encased in Mg block) were added to the Mg melt and hold for 30 min to ensure that Zn and Ca get melted and diffused sufficiently. The melt was heated up to 993 K and kept for 20 min, and then cast into a steel mould. The alloy prepared by traditional method was labeled as Alloy A. Small quantity of Alloy A was re-melted in a quartz tube filled with high-purity 99.999% argon (volume fraction), and then injected into a water-cooled copper mould by high-pressure argon. The acquired alloy was marked as Alloy B with dimensions of 80 mm × 15 mm × 2 mm. The preparation process is illustrated in Fig. 1.

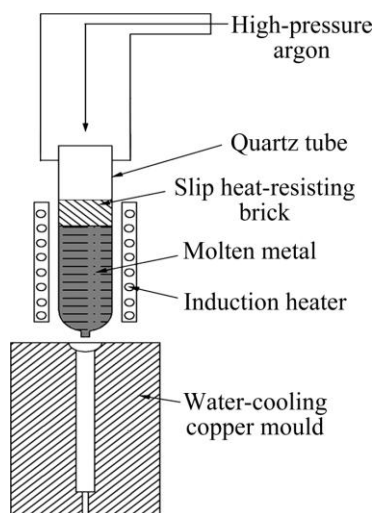


Fig. 1 Preparation process of Alloy B

Samples for microstructure observation and mechanical testing were cut from the ingots of Alloys A and B. The microstructure was observed by optical microscope (Olympus-GX71), and scanning electron microscope (SEM, Hitachi-S4800) equipped with an energy dispersive spectrometer (EDS). Phase analysis was conducted by X-ray diffraction (XRD, Bruker-D8).

Mechanical testing samples had a gauge length of 15 mm, width of 5 mm and a thickness of 2 mm. Tensile test was performed on INSTRON–5569 (static load cell  $\pm 5$  kN) tensile machine with a displacement rate of 1 mm/min at room temperature. Tensile strain curves were recorded by video extensometer with resolution of 1  $\mu$ m. Each alloy was tested for at least three samples.

For corrosion testing, samples of size 10 mm × 10 mm × 2 mm were polished stepwise up to 4000 grit, and then cleaned with acetone and dried with hot air. Polarization and immersion test were conducted in 3.5% NaCl and Hank's solution prepared with bi-distilled water and high-purity chemicals. Hank's solution preparation was according to Ref. [15] and its composition is listed in Table 1.

Table 1 Chemical composition of Hank's solution (mg/L)

NaCl	KCl	Na <sub>2</sub> HPO <sub>4</sub>	KH <sub>2</sub> PO <sub>4</sub>
8000	400	48	60
MgSO <sub>4</sub> ·7H <sub>2</sub> O	CaCl <sub>2</sub>	NaHCO <sub>3</sub>	
200	140	350	

Polarization test samples were mounted in epoxy resin with only 1 cm<sup>2</sup> surface area exposed. The electrolyte volumes of 3.5% NaCl and Hank's solutions were 500 mL and they were kept at 37 °C in water bath. Electrochemical measurements were carried out in a three-electrode system with a scan rate of 0.1 mV/s, which consist of a saturated calomel electrode as the reference electrode, a platinum electrode as the counter and the sample as the working electrode. The polarization measurements started at –2.0 V below the open circuit potential after the samples had been immersed in the solution for 5 min and corrosion potential  $\phi_{\text{corr}}$  and corrosion current density  $J_{\text{corr}}$  were obtained through LK9805 measurement system. All potentials were referred to the SCE and each experiment was repeated twice to check the reproducibility of the results.

The alloy specimens were immersed in 3.5% NaCl and Hank's solution respectively at 37 °C for 30 h, and then corrosion product was analyzed by XRD and EDS. In mass loss immersion test, the volume of Hank's solution was 800 mL and the solution was kept at 37 °C. The alloy specimens were weighed and then immersed in Hank's solution. After 120 h, they were cleaned with chromate acid for 5 min to remove the corrosion products and were weighed again. The corrosion rates were obtained by

$$R = m / (At)$$

where  $R$  is the corrosion rate (g/(cm<sup>2</sup> h));  $m$  is the weight loss (g),  $A$  is the sample area exposed to solution (cm<sup>2</sup>), and  $t$  is the exposure time (h) [16].

### 3 Results and discussion

#### 3.1 Microstructure

Optical microstructures of Alloys A and B are shown in Fig. 2. Coarse columnar structure is the main solidification morphology of Alloy A, as seen in Fig. 2(a) and grain size is over several hundred microns. For Alloy B seen in Fig. 2(b), fine equiaxed dendrites form and the size is about 20  $\mu\text{m}$ . The grain refinement is observably significant via raising cooling rate. Figure 3 shows the XRD results of two alloys and only  $\alpha$ -Mg phase can be detected.

Phase morphology is further analyzed by SEM. In Fig. 4(a), it can be found that bright latticed-shape

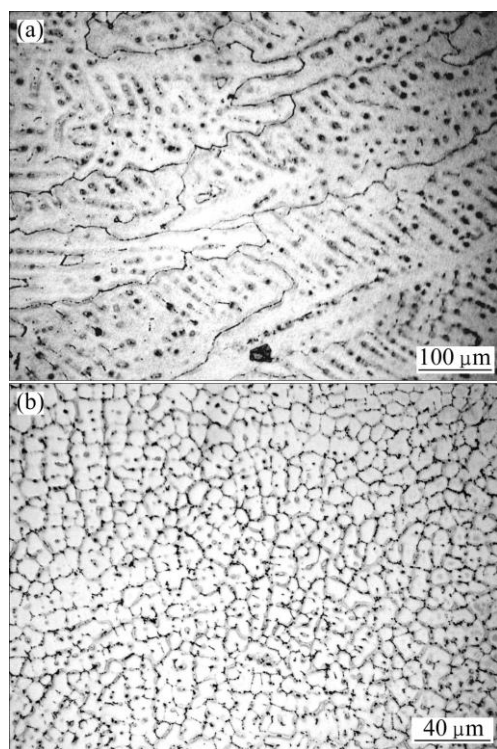


Fig. 2 Optical microstructures of Alloy A (a) and Alloy B (b)

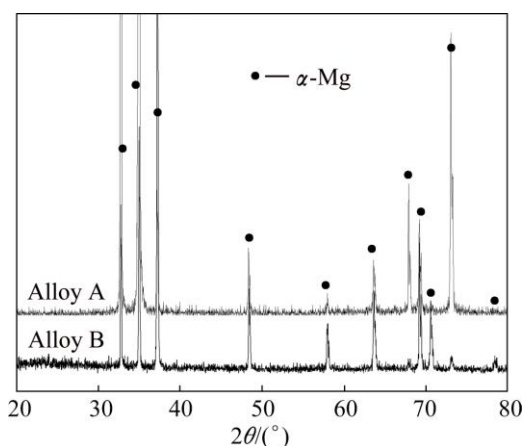


Fig. 3 XRD results of two alloys

substance distributes in inner grain. At a higher magnification in Fig. 4(b), it can be found that the latticed-shape substance contains two different parts. One is alloying element segregation in matrix and presents white color in backscattered electron image. Select a spot A in the above white region and the chemical composition is identified by EDS. The result shows that the white region contains excessive Zn in Fig. 4(c). It can be confirmed that Zn element is segregated and forms Zn-enrichment region in solid solution. The other is a lot of finer particles-like second phases which disperse homogeneously and the size is dozens of nanometers. It is reported [17,18] that the size, morphology and distribution of the second phase are changed greatly in Mg–Zn alloys when Ca element is added and a new kind of precipitate phase  $\text{Mg}_6\text{Zn}_3\text{Ca}_2$  is found. A lot of previous studies confirmed that three different phase reactions were detected in the low-alloyed Mg–Ca–Zn alloy system:  $\alpha$ -Mg,  $\text{Mg}_2\text{Ca}$  and  $\text{Mg}_6\text{Zn}_3\text{Ca}_2$ . ZHANG and YANG [19] reported that eutectic phase ( $\alpha$ -Mg+ $\text{Mg}_2\text{Ca}$ + $\text{Mg}_6\text{Zn}_3\text{Ca}_2$ ) was formed when alloy's composition Zn/Ca mole ratio was less than 1.0:1–1.2:1 and eutectic phase ( $\alpha$ -Mg +  $\text{Mg}_6\text{Zn}_3\text{Ca}_2$ ) was formed when alloy's composition Zn/Ca mole ratio was more than 1.0:1–1.2:1. BAKHSHEHI-RAD et al [20] further determined the forming temperature point of above three phases and above-mentioned critic point of alloy's composition, Zn/Ca mole ratio, was 1.23:1 in the Mg–0.5Ca–xZn alloy system. In the present study, second phase peaks are weaker and might be hidden in background noise in the XRD results of alloys in Fig. 3. The reason should be that the quantity of second phase is too small to be detected. In Fig. 4(d), the EDX results of the particles-like phase show that it was composed of Mg, Zn and Ca elements, 97.61%, 0.68% and 1.71% respectively. It can be confirmed that the phase contains  $\text{Mg}_6\text{Zn}_3\text{Ca}_2$ . The mole ratio of Ca/Zn was 2.5:1, which is more than the Ca/Zn mole ratio of 1.5:1 of  $\text{Mg}_6\text{Zn}_3\text{Ca}_2$ . The surplus Ca can confirm the existence of  $\text{Mg}_2\text{Ca}$  phase. According to previous studies and above discussion, the particle-like phase can be confirmed eutectic phase ( $\alpha$ -Mg+ $\text{Mg}_2\text{Ca}$ + $\text{Mg}_6\text{Zn}_3\text{Ca}_2$ ).

For Alloy B in Fig. 5, above bright latticed-shape substance is not obvious in inner grain in backscattered electron image. In Fig. 5(b) of higher magnification image, the particles-like phases are not found and only a few gray areas are observed. Select a spot C in the above gray areas and the chemical composition is identified by EDS. The results show that gray area is also segregated Zn element enrichment region in Fig. 5(c). Due to raising cooling rate, massive eutectic phase does not have enough time to precipitate during solidification process. Similarly, Zn atoms do not have enough time to be segregated and have been solvated in the matrix during

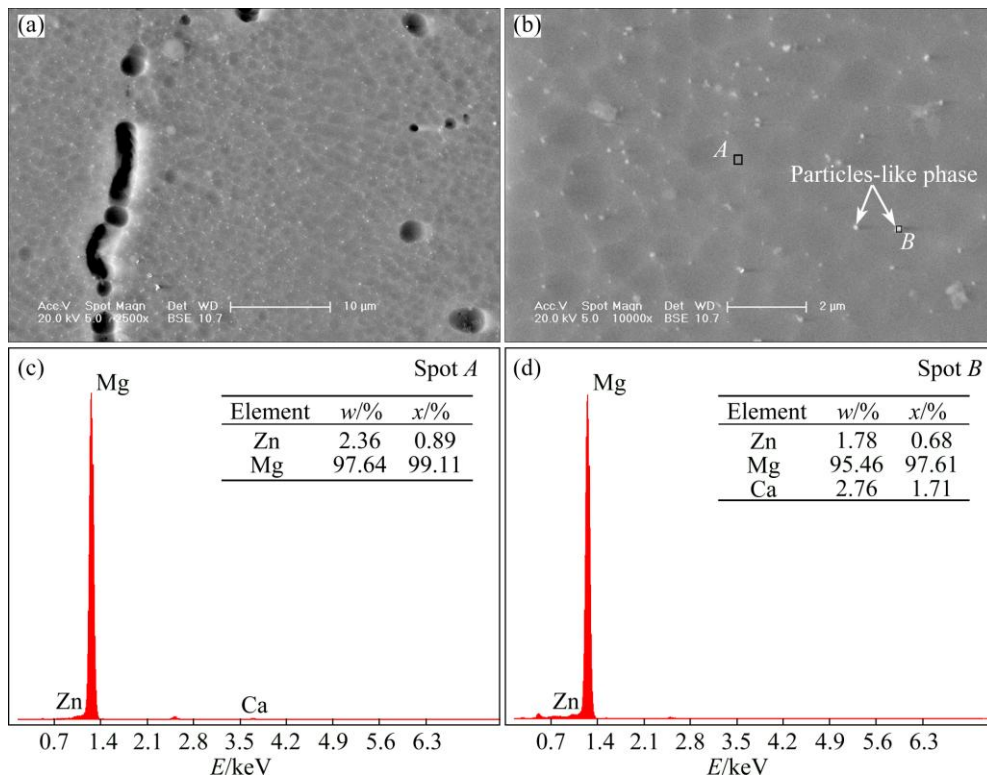


Fig. 4 SEM images (a, b) and EDS results (c, d) of Alloy A

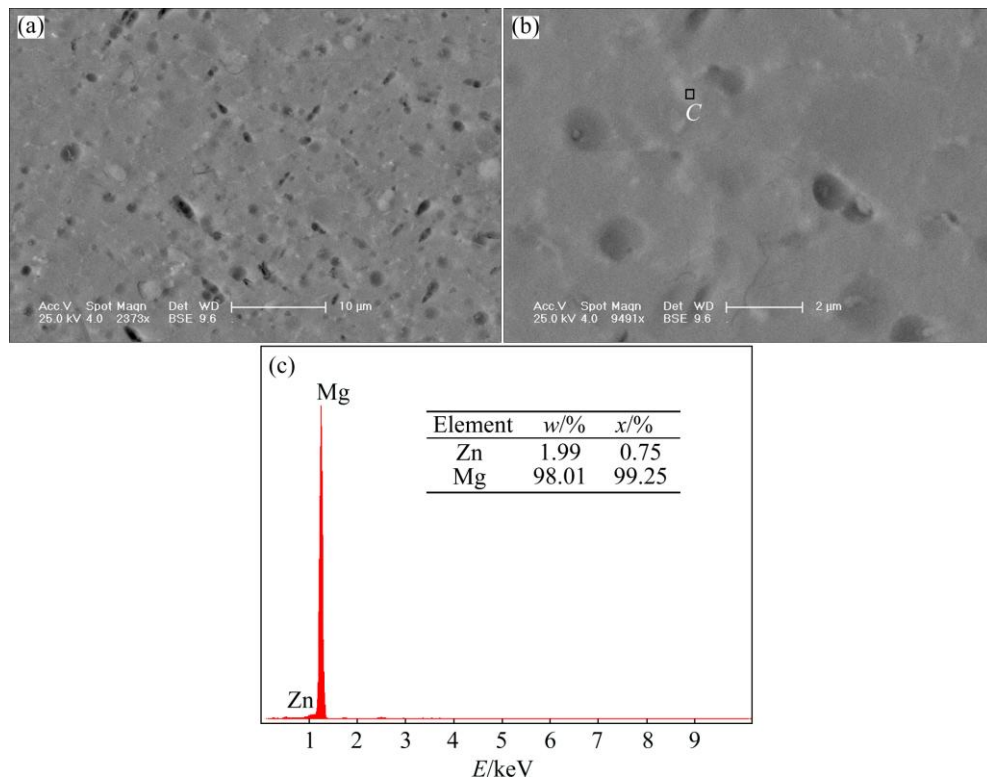


Fig. 5 SEM images (a, b) and EDS results (c) of Alloy B

solidification process. Thus, quantity of Zn enrichment regions is less than that of Alloy A. Most Zn and Ca atoms have been solid-solvated homogeneously in the matrix. In conjunction with grain size, it can be

confirmed that raising cooling rate can bring about microstructural refinement and homogeneity, and increase the solid solubility of alloying elements into the magnesium matrix.

### 3.2 Bio-corrosion properties

The electrochemical polarization curves of different samples in 3.5% NaCl and in Hank's solutions are shown in Fig. 6. The corrosion current density ( $J_{\text{corr}}$ ), corrosion potential ( $\phi_{\text{corr}}$ ), cathodic Tafel slopes ( $\beta_c$ ), anodic Tafel slopes ( $\beta_a$ ) from the polarization curves are shown in Table 2. The polarization resistance ( $R_p$ ) was calculated according to the following equation [21]:

$$R_p = \frac{\beta_a \beta_c}{2.3(\beta_a \beta_c) J_{\text{corr}}} \quad (1)$$

It can be seen that  $\phi_{\text{corr}}$  values of Alloy B both in 3.5% NaCl and in Hank's solution are more positive than those of Alloy A, indicating that Alloy B has better corrosion resistant tendency. In 3.5% NaCl, the  $J_{\text{corr}}$  of Alloy B is 5.47 mA/cm<sup>2</sup>, which is a little lower than that of Alloy A. In Hank's solution, the  $J_{\text{corr}}$  of Alloy B is obviously lower than that of Alloy A, which is 8.24 mA/cm<sup>2</sup> and is about 1/3 as low as that of Alloy A. From the calculated results of  $R_p$  value, Alloy B is higher than Alloy A both in 3.5% NaCl and in Hank's solutions. It can be concluded on the basis of data that Alloy B has better bio-corrosion resistance than Alloy A both in 3.5% NaCl and in Hank's solutions.

Figure 7 illustrates the surface morphologies of two alloys after the electrochemical tests in 3.5% NaCl and in Hank's solutions. In Figs. 7(a) and (b), separately showing surface morphology of two alloys in 3.5% NaCl, it can be found that the flake-like corrosion products cover on the surfaces of both Alloys A and B after the electrochemical tests. However, more seriously, corroded

morphology is observed on the surface of Alloy A with thick and long flakes. On the contrary, the flakes on Alloy B are thin and short. A lot of big and bright serious corrosion areas are found on the surface of Alloy A, while corrosion is reduced and alleviated on Alloy B surface. The surface morphologies of two alloys after the electrochemical tests in Hank's solution are illustrated separately in Figs. 7(c) and (d). In Alloy A, large corrosion spot is found and a lot of bright particle-like corrosion products disperse homogeneously on the surface. In Alloy B, the large corrosion spot is not found and the quantity of bright particles-like corrosion products decreases.

Figure 8 shows the XRD result of corrosion product of two alloy specimens after being immersed in 3.5% NaCl and Hank's solutions. The peaks of two alloys are consistent in both types of solution. It indicates that corrosion product of 3.5% NaCl immersion is mainly Mg(OH)<sub>2</sub> and during the corrosion the following chemical reactions occur ( $\text{Mg} \rightarrow \text{Mg}^{2+} + 2\text{e}^-$ ;  $\text{H}_2\text{O} + 2\text{e}^- \rightarrow \text{H}_2 + 2\text{OH}^-$ ;  $\text{Mg}^{2+} + 2\text{OH}^- \rightarrow \text{Mg}(\text{OH})_2$ ). However, phase peaks of corrosion product of Hank's solution immersion are weak and difficult to be determined. The corroded surfaces are further analyzed by EDS and the results show that corrosion product should contain O, P, Ca, Zn and Mg elements (seen in Fig. 9). KUWAHARA et al [22] pointed out that corrosion product on pure Mg immersed in Hank's solution was amorphous magnesium-substituted apatite  $(\text{Ca}_{0.86}\text{Mg}_{0.14})_{10}(\text{PO}_4)_6(\text{OH})_2$ . LI et al [4] suggested that a mixture of Mg(OH)<sub>2</sub> and hydroxyapatite (HA,  $\text{Ca}_{10}(\text{PO}_4)_6(\text{OH})_2$ ) formed on

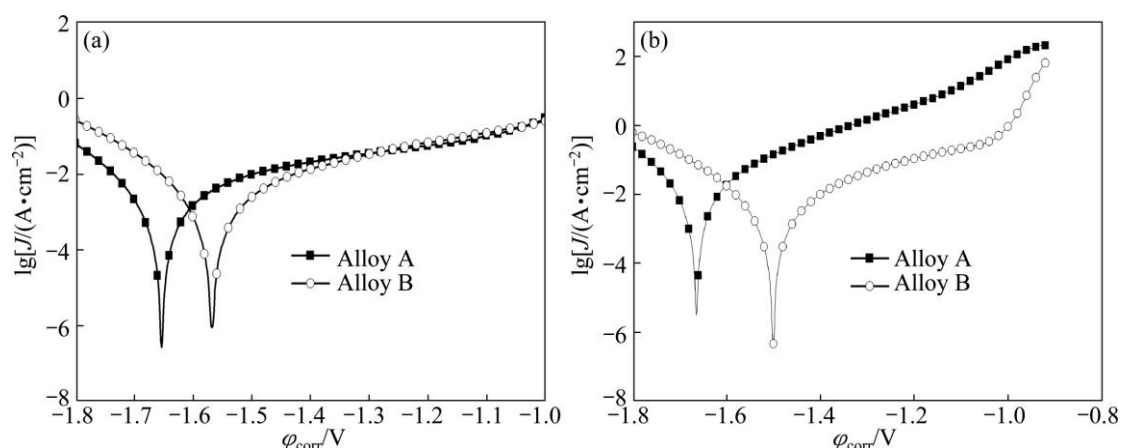
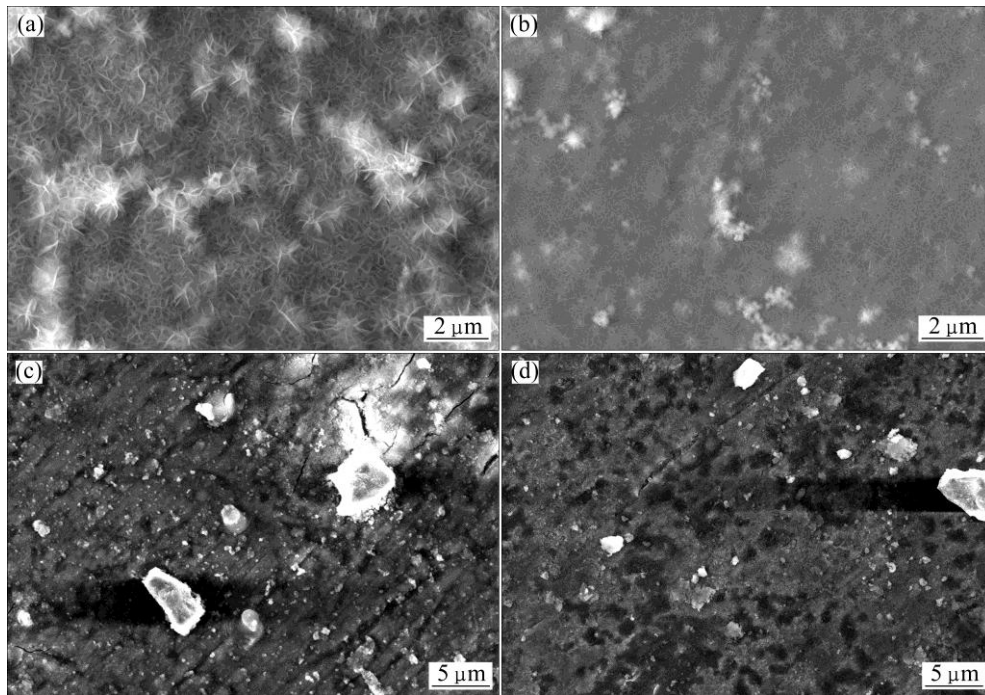


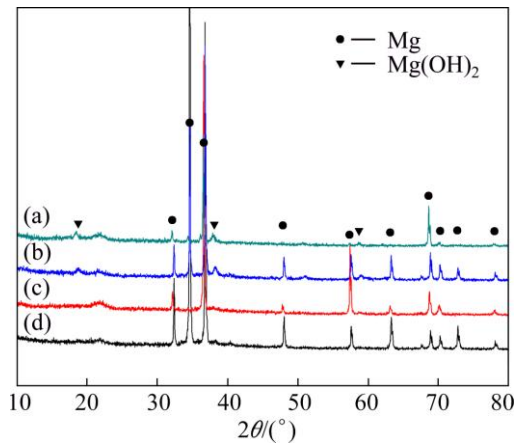
Fig. 6 Electrochemical polarization curves of different samples: (a) In 3.5% NaCl; (b) In Hank's solution

Table 2 Electrochemical data and immersion corrosion rate of different samples

Sample	Electrolyte	$\phi_{\text{corr}}/\text{mV}$	$J_{\text{corr}}/(\text{mA cm}^{-2})$	$\beta_a/(\text{V decade}^{-1})$	$\beta_c/(\text{V decade}^{-1})$	$R_p/\text{k}\Omega$	$R/(\text{g cm}^{-2} \text{h}^{-1})$
Alloy A	3.5% NaCl	-1654	6.86	2.03	-7.60	0.102	
Alloy B		-1568	5.47	2.93	-7.46	0.178	
Alloy A	Hank's solution	-1665	24.04	4.82	-7.47	0.053	$26.4 \times 10^{-5}$
Alloy B		-1501	8.24	3.64	-6.36	0.122	$6.79 \times 10^{-5}$



**Fig. 7** Surface morphologies of two alloys after electrochemical tests in different solutions: (a) Alloy A, in 3.5% NaCl; (b) Alloy B, in 3.5% NaCl; (c) Alloy A, in Hank's solution; (d) Alloy B, in Hank's solution



**Fig. 8** XRD patterns of corrosion product of two alloys after immersion for 30 h in different solutions: (a) Alloy A, in 3.5% NaCl; (b) Alloy B, in 3.5% NaCl; (c) Alloy A, in Hanks' solution; (d) Alloy B, in Hanks' solution

the surface of Mg–1Ca alloy with long immersion time in simulated body fluid (SBF). ZHANG et al [5] reported that corrosion products should contain hydroxyapatite,  $\text{Mg}(\text{OH})_2$  and other Mg/Ca phosphates on the surface of Mg–Zn alloy immersed in simulated body fluid (SBF). There is no consistent conclusion. Considering that the ions concentration of Hank's solution used in this study is close to that of simulated body fluid (SBF), we think that complicated chemical reactions occur among phosphate ions ( $\text{H}_2\text{PO}_4^-$ ,  $\text{HPO}_4^{2-}$  or  $\text{PO}_4^{3-}$ ),  $\text{Ca}^{2+}$ ,  $\text{Mg}^{2+}$  and  $\text{OH}^-$  in Hanks' solution immersion and corrosion product should be complex mixture containing HA.

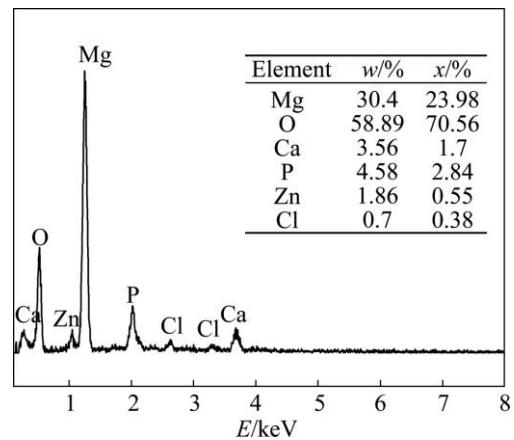


**Fig. 9** EDS results of corrosion product of Hank's solution immersion

The corrosion rates of Alloys A and B after 120 h Hanks' solution immersion are  $26.4 \times 10^{-5}$  and  $6.79 \times 10^{-5}$   $\text{g}/(\text{cm}^2 \text{h})$ , respectively and listed in Table 2. The corrosion rate of Alloy B is much slower than that of Alloy A and is about 1/4 that of the Alloy A. From above immersion test results, corrosion resistance of Alloy B is superior to that of Alloy A both in 3.5% NaCl and in Hank's solutions, which is in agreement with the electrochemical test. Alloy B has more refined and homogeneous microstructure due to preparation by raising cooling rate, which leads to chemical homogeneity and in turn enhances corrosion resistance. Previous studies [19] reported that the electrochemical potentials of the phases are as follows:  $\text{Mg}_6\text{Zn}_3\text{Ca}_2 >$

$\alpha$ -Mg>Mg<sub>2</sub>Ca. Eutectic phase of Alloy A is composed of  $\alpha$ -Mg, Mg<sub>2</sub>Ca and Mg<sub>6</sub>Zn<sub>3</sub>Ca<sub>2</sub>. At the beginning, Mg<sub>6</sub>Zn<sub>3</sub>Ca<sub>2</sub> phase acts as cathode and Mg<sub>2</sub>Ca phase acts as anode, and Mg<sub>2</sub>Ca phase is corroded faster than  $\alpha$ -Mg and Mg<sub>6</sub>Zn<sub>3</sub>Ca<sub>2</sub>. After Mg<sub>2</sub>Ca phase is corroded off, new galvanic couple occurs, and Mg<sub>6</sub>Zn<sub>3</sub>Ca<sub>2</sub> acts as cathode and  $\alpha$ -Mg phase acts as anode. The Mg<sub>6</sub>Zn<sub>3</sub>Ca<sub>2</sub> remains while  $\alpha$ -Mg phase around Mg matrix is corroded. Similarly, there are electrochemical potentials between Zn enrichment region Mg matrix, and micro anode-cathode sites form in Alloy A as well. Thus, more eutectic phases and Zn enrichment regions cause more serious corrosion. For Alloy B, grain refinement is significant and will result in the increase of the amount of grain boundary, which is detrimental to the corrosion resistance of the alloy. However, eutectic phase ( $\alpha$ -Mg + Mg<sub>2</sub>Ca + Mg<sub>6</sub>Zn<sub>3</sub>Ca<sub>2</sub>) has no time to precipitate and Zn atoms have not enough time to be segregated and form less enrichment regions in the matrix by raising cooling rate. Reduction of micro anode-cathode sites leads to alleviate corrosion and the corrosion resistance of Alloy B is improved. Microstructure homogeneity and micro-galvanic corrosion alleviation are the reasons of corrosion resistance improvement of Alloy B.

### 3.3 Mechanical properties

Typical stress–strain curves of Alloys A and B at room temperature are shown in Fig. 10 and corresponding mechanical properties are listed in Table 3. The ultimate tensile strength and yield strength of Alloy A are 125.2 MPa and 38.2 MPa, respectively. The ultimate tensile strength and yield strength of Alloy B increase remarkably. The values of ultimate tensile strength and yield strength are 194.4 and 85.6 MPa, which are 1.55 times and 2.24 times to those of Alloy A, respectively. Compared to Alloy A, elongation of Alloy B improves from 7.8% to 14.9%. Grain size and precipitation are two factors influencing mechanical properties of two alloys. For Alloy A, the fine second eutectic phase precipitates are beneficial to enhance mechanical properties. However, the gains size of Alloy B is reduced about dozens of times than that of Alloy A. The Hall–Petch relationship [23] ( $\sigma_y = \sigma_0 + k_y d^{-1/2}$ , where  $\sigma_0$  and  $k_y$  are constants for a particular material), which describes the functional relationship between the yield strength  $\sigma_y$  and the average grain diameter  $d$ , has been universally applied to many materials. A fine-grained material is harder and stronger than the coarse one. The fine-grained materials have greater total grain boundary, which can effectively hind basal plane slip and inhibit the deformation under mechanical stress. Thus, grain refinement is the main reason for the improvement of mechanical properties of Alloy B.

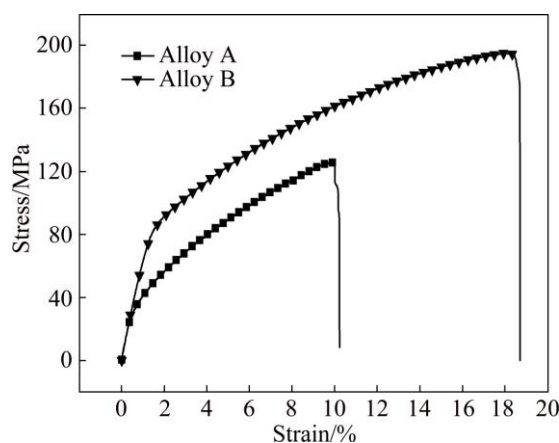


Fig. 10 Typical stress–strain curves of Alloys A and B

Table 3 Mechanical properties of Alloys A and B

Alloy	YS ( $\sigma_{0.2}$ )/MPa	UTS ( $\sigma_b$ )/MPa	$\epsilon$ /%
Alloy A	38.2	125.2	7.8
Alloy B	85.6	194.4	14.9

## 4 Conclusions

1) Eutectic phase ( $\alpha$ -Mg+Mg<sub>2</sub>Ca+Mg<sub>6</sub>Ca<sub>2</sub>Zn<sub>3</sub>) and Zn element enrichment regions were found in micrographs of Mg–1Zn–0.5Ca alloy prepared by traditional steel mould casting. Grain size was remarkably reduced by raising cooling rate. Zn element enrichment regions were observably reduced and above eutectic phases were not found via raising cooling rate.

2) The alloy prepared by water-cooled copper mould injection casting has more positive  $\phi_{\text{corr}}$ , lower  $J_{\text{corr}}$  and higher  $R_p$  value than by traditional steel mould casting both in 3.5% NaCl and in Hank's solutions. The corrosion rate of the former is about 1/4 that of the latter in mass loss immersion test. The electrochemistry and immersion corrosion tests results indicated that raising cooling rate can improve corrosion resistance both in 3.5% NaCl and Hank's solutions. It is because more homogeneous microstructure can be obtained by raising cooling rate, which leads to chemical homogeneity and micro-galvanic corrosion alleviation.

3) The yield strength, ultimate tensile strength and elongation of the alloy were also improved by raising cooling rate. Grain refinement is the main reason for the improvement.

## References

- [1] WITTE F. The history of biodegradable magnesium implants: A review [J]. Acta Biomaterialia, 2010, 6: 1680–1692.
- [2] KUBÁSEK J, VOJTĚCH D. Structural and corrosion characterization of biodegradable Mg–RE (RE=Gd, Y, Nd) alloys [J]. Transactions of Nonferrous Metals Society of China, 2013, 23(5):

- 1215–1225.
- [3] ZHANG E L, YIN D L, XU L P, YANG L, YANG K. Microstructure, mechanical and corrosion properties and biocompatibility of Mg–Zn–Mn alloys for biomedical application [J]. *Materials Science and Engineering C*, 2009, 29: 987–993.
- [4] LI Z J, GU X N, LOU S Q, ZHENG Y F. The development of binary Mg–Ca alloys for use as biodegradable materials within bone [J]. *Biomaterials*, 2008, 29: 1329–1344.
- [5] ZHANG S X, LI J N, SONG Y, ZHAO C L, ZHANG X N, XIE C Y, ZHANG Y, TAO H R, HE Y H, JIANG Y, BIAN Y J. In vitro degradation, hemolysis and MC3T3-E1 cell adhesion of biodegradable Mg–Zn alloy [J]. *Materials Science and Engineering C*, 2009, 29: 1907–1912.
- [6] ZHANG S X, ZHANG X N, ZHAO C L, LI J N, SONG Y, XIE C Y, TAO H R, ZHANG Y, HE Y H, JIANG Y, BIAN Y J. Research on an Mg–Zn alloy as a degradable biomaterial [J]. *Acta Biomaterialia*, 2010, 6: 626–640.
- [7] ZANDER D, ZUMDICK N A. Influence of Ca and Zn on the microstructure and corrosion of biodegradable Mg–Ca–Zn alloys [J]. *Corrosion Science*, 2015, 93: 222–233.
- [8] GENG L, ZHANG B P, LI A B, DONG C C. Microstructure and mechanical properties of Mg–4.0Zn–0.5Ca alloy [J]. *Materials Letters*, 2009, 63: 557–559.
- [9] BAKHSHESHI-RAD H R, IDRIS M H, ABDUL KADIR M R, DAROONPARVAR M. Effect of fluoride treatment on corrosion behavior of Mg–Ca binary alloy for implant application [J]. *Transactions of Nonferrous Metals Society of China*, 2013, 23(3): 699–710.
- [10] GU X N, ZHENG W, CHENG Y, ZHENG Y F. A study on alkaline heat treated Mg–Ca alloy for the control of the biocorrosion rate [J]. *Acta Biomaterialia*, 2009, 5: 2790–2799.
- [11] WANG H X, GUAN S K, WANG X, REN C X, WANG L G. In vitro degradation and mechanical integrity of Mg–Zn–Ca alloy coated with Ca-deficient hydroxyapatite by the pulse electrodeposition process [J]. *Acta Biomaterialia*, 2010, 6: 1743–1748.
- [12] WANG Jing-feng, HUANG Song, GUO Sheng-feng, WEI Yi-yun, PAN Fu-sheng. Effects of cooling rate on microstructure, mechanical and corrosion properties of Mg–Zn–Ca alloy [J]. *Transactions of Nonferrous Metals Society of China*, 2013, 23(7): 1930–1935.
- [13] YAMASAKI M, IZUMI S, KAWAMURA Y, HABAZAKI H. Corrosion and passivation behavior of Mg–Zn–Y–Al alloys prepared by cooling rate-controlled solidification [J]. *Applied Surface Science*, 2011, 257: 8258–8267.
- [14] LIU De-bao, LIU Yi-chi, HUANG Yan, SONG Rong, CHEN Min-fang. Effects of solidification cooling rate on the corrosion resistance of Mg–Zn–Ca alloy [J]. *Progress in Natural Science: Materials International*, 2014, 24: 452–457.
- [15] HANKS J H, WALLACE R E. Relation of oxygen and temperature in the preservation of tissues by refrigeration [J]. *Bulletin of Experimental Biology and Medicine*, 1949, 71: 196–200.
- [16] ASTM-G31-72. Standard practice for laboratory immersion corrosion testing of metals [S].
- [17] LARIONOVA T V, PARK W W, YOU B S. A ternary phase observed in rapidly solidified Mg–Ca–Zn alloys [J]. *Scripta Materialia*, 2001, 45: 7–12.
- [18] LEVI G, AVRAHAM S, ZILBEROV A, BAMBERGER M. Solidification, solution treatment and age hardening of a Mg–1.6wt.%Ca–3.2wt.%Zn alloy [J]. *Acta Materialia*, 2006, 54: 523–530.
- [19] ZHANG E L, YANG L. Microstructure, mechanical properties and bio-corrosion properties of Mg–Zn–Mn–Ca alloy for biomedical application [J]. *Materials Science and Engineering A*, 2008, 497: 111–118.
- [20] BAKHSHESHI-RAD H R, ABDUL-KADIR M R, IDRIS M H, FARAHANY S. Relationship between the corrosion behavior and the thermal characteristics and microstructure of Mg–0.5Ca–xZn alloys [J]. *Corrosion Science*, 2012, 64: 184–197.
- [21] ARGADE G R, KANDASAMY K, PANIGRAHI S K, MISHRA R S. Corrosion behavior of a friction stir processed rare-earth added magnesium alloy [J]. *Corrosion Science*, 2012, 58: 321–326.
- [22] KUWAHARA H, AL-ABDULLAT Y, MAZAKI N, TSUTSUMI S, AIZAWA T. Precipitation of magnesium apatite on pure magnesium surface during immersing in Hank's solution [J]. *Materials Transactions* 2001, 42: 1317–1321.
- [23] CALLISTER W D. *Fundamentals of materials science and engineering* [M]. 5th ed. Beijing: Chemical Industry Press, 2002.

## 冷却速率对铸造 Mg–1Zn–0.5Ca 合金 耐生物腐蚀性和力学性能的影响

王立东<sup>1,2</sup>, 李雪松<sup>3</sup>, 王超<sup>3</sup>, 王立民<sup>2</sup>, 曹占义<sup>1</sup>

1. 吉林大学 材料科学与工程学院, 汽车材料教育部重点实验室, 长春 130025;
2. 中国科学院 长春应用化学研究所, 稀土资源利用国家重点实验室, 长春 130022;
3. 长春工业大学 先进结构材料教育部重点实验室, 长春 130012

**摘要:** 采用传统钢模铸造法和高冷却速率的水冷铜模喷铸法两种方法制备 Mg–1Zn–0.5Ca 合金, 对合金的组织、力学性能和生物腐蚀性能进行对比研究。研究表明, 提高冷却速度, 合金的组织更均匀, 晶粒尺寸显著细化。在 3.5% NaCl 溶液和模拟体液 Hank's 溶液中采用动电位极化和浸泡失重测试合金的耐生物腐蚀性, 结果显示高冷却速率下制备的合金在两种溶液中均具有较好的耐生物腐蚀性, 其原因为提高冷却速率使合金组织更均匀, 原电池腐蚀效应减弱。提高冷却速度, 合金的屈服强度、抗拉强度和伸长率等力学性能得到提高。晶粒细化是其力学性能提高的主要原因。

**关键词:** Mg–1Zn–0.5Ca 合金; 冷却速率; 耐生物腐蚀性; 原电池腐蚀; 力学性能

(Edited by Yun-bin HE)